TITLE PAGE

Citation Format:

Heidrun Wabnitz, Mikhail Mazurenka, Katja Fuchs, Laura Di Sieno, Gianluca Boso, Davide Contini, Alberto Dalla Mora, Alberto Tosi, Yoko Hoshi, Antonio Pifferi, Rainer Macdonald, "Non-contact scanning time-domain functional optical imaging of the adult human brain," Diffuse Optical Imaging V, edited by Hamid Dehghani, Paola Taroni, Proc. of SPIE Vol. 9538, 953802

Copyright notice:

DOI abstract link:

http://dx.doi.org/10.1117/12.2183288

Non-contact scanning time-domain functional optical imaging of the adult human brain

Heidrun Wabnitz*[a], Mikhail Mazurenka[a,b], Katja Fuchs[a], Laura Di Sieno[c], Gianluca Boso[d], Davide Contini[c], Alberto Dalla Mora[c], Alberto Tosi[d], Yoko Hoshi[e], Antonio Pifferi[c], Rainer Macdonald[a]

[a]Physikalisch-Technische Bundesanstalt (PTB), Abbestraße 2-12, 10587 Berlin, Germany; [b]Hannoversches Zentrum für Optische Technologien, Nienburger Str. 17, 30167 Hannover, Germany; [c]Politecnico di Milano, Dipartimento di Fisica, Piazza Leonardo da Vinci 32, 20133 Milano, Italy; Milano, Italy; [d]Politecnico di Milano, Dipartimento di Elettronica, Informazione e Bioingegneria, Piazza Leonardo da Vinci 32, 20133 Milano, Italy; [e]Tokyo Metropolitan Institute of Medical Science, 2-1-6 Kamikitazawa, Setagaya-ku, Tokyo 156-8506, Japan

ABSTRACT

We developed a novel scanning system that relies on gated detection of late photons at short source-detector separation, enabling the recording of absorption changes in deep tissue compartments. The tissue was scanned by a galvanometer scanner from a distance of more than 10 cm, with a fixed separation of the illumination and the detection spot of a few mm. The light source was a supercontinuum laser with an acousto-optic tunable filter that was used to rapidly switch between two wavelength bands centered at 760 nm and 860 nm. A fast-gated single-photon avalanche diode was employed to eliminate the intense early part of the diffusely remitted signal and to detect photons with long times of flight with improved signal-to-noise ratio. A second detection channel contained a non-gated detector. The gated and non-gated time-of-flight distributions of photons were recorded by imaging time-correlated single photon counting synchronized with the movement of the scanner. A tissue area with dimensions of several cm was scanned with 32×32 pixels within a frame time of 1 s. Sensitivity and spatial resolution of the system were characterized by phantom measurements. In-vivo tests included functional brain activation by various tasks and demonstrated the feasibility of non-contact imaging of hemodynamic changes in the cerebral cortex.

Keywords: diffuse optical imaging, time-domain optical brain imaging, fast-gated detector, tissue-like phantoms, brain activation, fNIRS, scanning

1. INTRODUCTION

During twenty years of development of functional near-infrared spectroscopy (fNIRS) of the brain, numerous approaches and technical solutions have been reported, among them continuous wave (CW) optical topography and tomography employing multiple sources and detectors or time-domain fNIRS imaging[1]. While these techniques usually rely on direct contact between fiber-based optodes and the tissue surface, there is a trend towards non-contact approaches. They allow problems to be avoided that arise from pressure and unstable coupling between the optodes and the skin. Another advantage of non-contact approaches is the opportunity to obtain images that contain a larger number and more densely spaced pixels compared to arrays of multiple optodes.

A specific development for time-resolved diffuse reflectance measurements for the characterization of deep tissue compartments is the null source-detector separation approach[2] in conjunction with a single-photon avalanche diode (SPAD) operated in fast-gated mode[3]. By gating off early photons, late photons that visited deep tissue regions can be recorded with good signal-to-noise ratio.

The novel non-contact scanning approach described in this contribution combines the following features, i) non-contact imaging, ii) a dense and flexible grid of measurement positions, iii) depth-selective detection (up to a few cm depth) by time-resolved recording. Proof-of-principle tests of our non-contact method on phantoms were reported in Ref. 4. The implementation of a scanning setup and first *in vivo* tests were described Refs. 5 and 6. To achieve depth selectivity, i.e. a separation between absorption changes in the brain and superficial tissues, the recording of late photons needs to be combined with the information carried by early photons. Here we report on an upgraded and optimized scanning setup

Diffuse Optical Imaging V, edited by Hamid Dehghani, Paola Taroni, Proc. of SPIE Vol. 9538, 953802 · © 2015 SPIE · CCC code: 1605-7422/15/$18 · doi: 10.1117/12.2183288

that also contains a second, non-gated channel. The optimized system was characterized by phantom measurements and applied in an *in-vivo* study with brain activation paradigms on healthy subjects.

2. SYSTEM ARCHITECTURE

The optical setup and the signal flow of the upgraded non-contact scanning system are shown in Fig. 1. A supercontinuum laser (SC500-6, Fianium Ltd, UK) equipped with an 8-channel acousto-optic tunable filter (AOTF) for the near-infrared spectral range provided picosecond pulses (< 100 ps) at a repetition rate of 40.5 MHz. To maximize the laser power transmitted by the AOTF, all its eight channels were stacked together, with a wavelength spacing (~4 nm) optimized for maximum output. By using the "FSK" (Frequency Shift Keying) mode a fast switching between two wavelength bands was achieved. These bands were chosen with their centers at 760 nm and 860 nm, respectively. The output beam of the AOTF was directed to the tissue by the mirrors of a 2-axis galvanometer scanner (ProSeries PS-20, Cambridge Technology Europe GmbH, Germany).

Light diffusely reemitted from the tissue passed the scanner again and was imaged onto a multimode fiber (diameter 200 µm, NA 0.48, length 2 m, entrance face angled by 8°; CeramOptec GmbH, Germany). The output face of the detection fiber was imaged onto the active area (100 µm diameter) of the SPAD detector by a pair of aspheric lenses. The optical system was designed such that reflections from the tissue surface as well as from optical components were suppressed as far as possible. This included the use of a polarization splitting cube that selected the polarization direction perpendicular to that of the laser beam. For the measurements reported here, the offset between illumination and detection spots (source-detector separation) was adjusted to 5 mm in y direction.

Selective detection of late photons was achieved with a second generation compact fast-gated SPAD module (Politecnico di Milano, Italy) with embedded gating and signal conditioning circuitry[7]. The gate delay was adjusted by a home-built transmission-line based delay generator with 25 ps steps. An imaging time-correlated single photon counting (TCSPC) module (SPC-150, Becker&Hickl, Germany) was used to record the gated time-of-flight distribution (DTOF) in each scan position. The data processing was based on a time-window (TW) analysis within the late-photon part of the DTOF that was selected by the electronic gate. The limits of this time window were defined such to include a part of the DTOF with a good signal-to-noise ratio while avoiding the influence of residual reflections in the optical path due to early photons. For further details see Ref. 5.

A second parallel detection channel was equipped with a free-running (non-gated) silicon SPAD (PFCCTB, Micro Photon Device S.r.l., Italy), to additionally measure superficial absorption changes. A glass plate inserted in the optical path reflected a small fraction of the light from the tissue into the graded index fiber connected to the SPAD. Its output was recorded with a second imaging TCSPC module SPC-150 (not shown in Fig. 1 for simplicity).

A scan controller card GVD-120 (Becker&Hickl, Germany) was employed to control the scan as well as the image acquisition. Scan parameters included the size and shape (square or rectangular) of the scan area and the acquisition time. Corresponding x and y ramp signals were applied to the galvanometer scanner. In parallel, the actual frame, line and pixel information was communicated to the imaging TCSPC modules (SPC-150, Becker&Hickl, Germany). The parameters were adjusted to cover a scan area of, e.g. 4×4 cm^2 on the tissue with a 32×32 pixel frame size in step scanning mode. The frame time was chosen to be 1 s, resulting in a pixel time of ~1 ms. The Laser Routing signal of the scan controller was applied to the FSK input of the AOTF to switch between the two wavelength bands (around 760 nm and 860 nm) from line to line. Thus for each frame two 32×16 pixel images corresponding to the two wavelengths were recorded quasi-simultaneously.

3. PERFORMANCE CHARACTERIZATION

The system was characterized by a set of phantom measurements according to the protocols developed in the "nEUROPt" project [8,9]. In particular, the responsivity of the detection system was measured to assess and optimize the optical system. To characterize the spatial resolution performance, measurements were carried out on inhomogeneous phantoms.

Responsivity of the detection system

The efficiency of the detection system is important for the capability of a diffuse optical instrument to detect small amounts of light emerging from tissue. The detection system of the scanning system consists of the free-space and fiber optics in the optical path from the tissue to the detector and the detector itself. The responsivity of the entire detection

system can be measured by means of a light source with known radiance and an angular distribution similar to that emerging from tissue. We measured the responsivity as described in Ref. 8, by means of a slab phantom of known diffuse transmittance factor. Such phantom was positioned beneath the scanner, with its exit surface in the x-y plane, and the detection spot centered. The laser light was coupled into a multimode fiber that was mounted underneath the slab phantom in touch with the center of the entrance surface. In this configuration, the count rate was measured for both wavelengths. The responsivity s_{det}^{L} was calculated by dividing the count rate by the power incident to the phantom and by the wavelength-dependent diffuse transmittance factor of the phantom[8].

After optimization of the whole system with respect to its detection efficiency, the following responsivity values were obtained: $0.039 \cdot 10^{-3}$ mm^2 sr at 760 nm and $0.018 \cdot 10^{-3}$ mm^2 sr at 860 nm. These values are by about 3 orders of magnitude smaller than those found for different fiber-based time-domain optical brain imagers. This difference can be explained by the smaller effective detection area (about 1 mm in diameter for the non-contact system), the much smaller acceptance angle, the loss due to the polarization-dependent detection and losses in imaging the output of the detection fiber onto the small active area of the fast-gated SPAD.

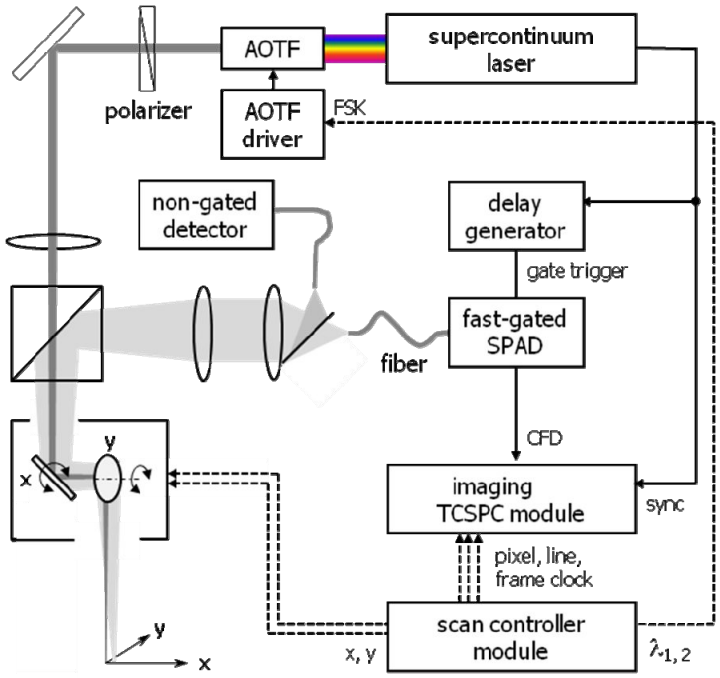

Figure 1. Schematic of the non-contact scanning system.

Depth-dependent sensitivity and lateral spatial resolution

We scanned an inhomogeneous phantom consisting of a turbid liquid and small solid black inclusions, as described in the implementation of the nEUROPt protocol[9]. The liquid was a mixture of Intralipid-20%, India ink and water. The optical properties of the liquid were estimated from the weights of the components and the scattering and absorption properties of Intralipid and ink[10]. The reduced scattering coefficient and the absorption coefficient were $\mu_s' = 0.84$ mm^{-1} and $\mu_a = 0.011$ mm^{-1}, respectively, at 760 nm. As inclusions, black plastic (polyvinyl chloride, PVC) cylinders were used with volumes of 25, 50, 100, 250, and 500 mm^3. They were held in upright position from underneath by a steel wire that was painted white. The use of black inclusions was motivated by the finding that totally absorbing inclusions of different size can mimic realistic absorption perturbations for a wide range of optical properties, geometries and operating conditions[11].

Fig. 2a illustrates the DTOFs recorded during the phantom measurement. Without applying the delayed gate, both curves would nearly coincide. Cutting off the early part of the DTOF by the gated detector permits to increase the laser power and thus the count rate for late photons. Fig. 2b depicts the contrast measured for the smallest cylinder (height = diameter

= 3.2 mm) as a function of depth z, for 760 nm. For $z = 0$ the upper surface of the cylinder was flush with the surface of the liquid. The contrast was defined as $C = 1 - N_{TW}/N_{TW,0}$ where N_{TW} is the photon count in the time window selected and $N_{TW,0}$ the baseline value far from the inclusion. It is evident that the measurement at late times provides a much higher contrast than at early times, in particular for $z > 5$ mm. At $z = 0$ the contrast is nearly 1 in both cases because there is virtually no scattering liquid between inclusion and surface. It should be noted that as long as the black inclusion is close to the surface, the equivalence relation for absorption perturbations[11] is not valid.

To assess lateral resolution, the region of maximum contrast was selected from the entire 2D scan. In Fig. 3 contrast curves as a function of x are plotted for various depths z for early and late photons. Spatial resolution as given by the full width at half maximum (FWHM) of the contrast curve exhibits only minor changes with depth. It increases from about 4 mm with the cylinder at the surface to 7 mm at $z = 6$ mm (see Fig. 3c). For late photons, the contrast curve exhibits marked wings at $z = 0$ already since the spatial sensitivity profile for late photons is more extended than that for early photons. There is a certain probability that they are influenced by the small inclusion even if it is located several mm away. When the inclusion is moved to increasing depth, the spatial resolution substantially decreases, as expected. For example, at $z = 6$ mm the FWHM reaches 14 mm.

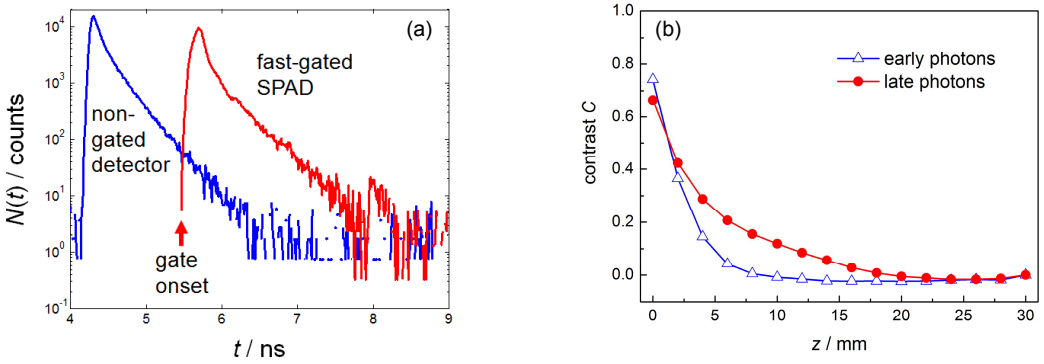

Figure 2. (a) DTOFs acquired by both detectors during the phantom measurement for a single pixel, for 100 frames added. (b) Depth-dependent contrast derived for both detection channels for the region of maximum contrast (3×3 pixels).

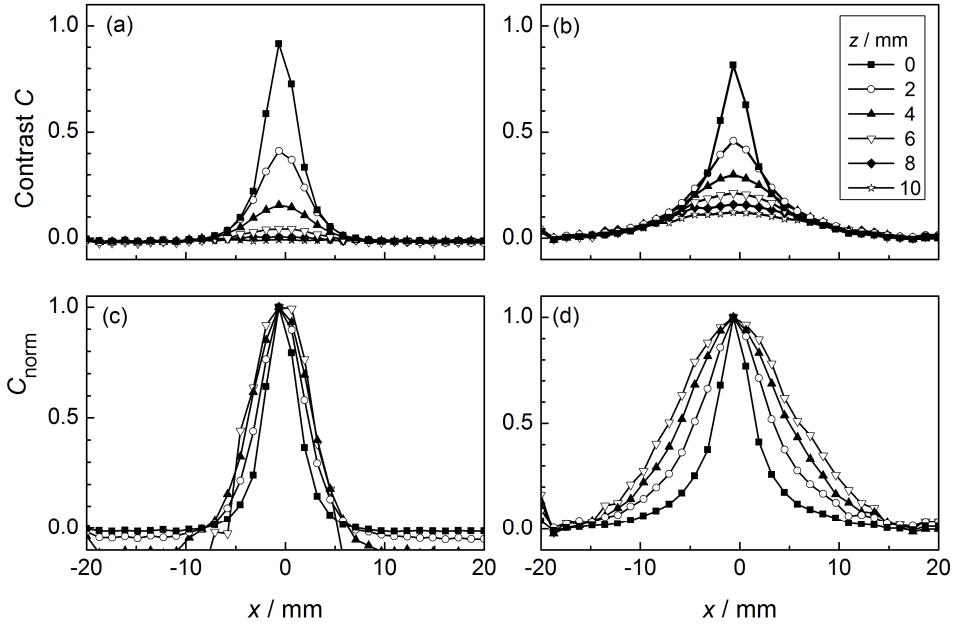

Figure 3. Lateral spatial resolution (at 760 nm) in x direction at various depths z of a small black cylinder of 25 mm^3 volume. Contrast (a, b) and normalized contrast (c, d) are plotted for early photons (a, c) and late photons (b, d).

4. *IN-VIVO* MEASUREMENTS: BRAIN ACTIVATION

The capability of the scanning system to measure brain activation was tested with various stimulation paradigms in healthy subjects, for details see Ref. 5. The motor stimulation experiment showed most clearly that a localized cerebral response could be detected. It should be noted that the measurement was pretty much impaired by the existence even of short hair. The measurement on the same almost entirely bald subject was repeated with the upgraded system, about 1.5 years later. Two motor stimulation paradigms were performed in the same session, (a) finger tapping (same as in Ref. 5), (b) handgrip by squeezing a soft ball. In both cases, the stimulation lasted 32 s, followed by 32 s of rest, with 20 repetitions. The results are illustrated in Fig. 4. The results related to both stimulation paradigms show a localized response. The increase in oxy- and decrease in deoxyhemoglobin during stimulation indicated a cerebral response. The finger tapping experiment exhibited a similar pattern as in the previous experiment[5]. In contrast, the hand grip experiment yielded a much more extended activation area. This is expected because additional parts of the motor cortex become involved when moving the hand. Furthermore, the sensory cortex is more activated during hand grip than during finger tapping. The signal-to-noise ratio is poor in the lower right corner of the image, a region where hair is present.

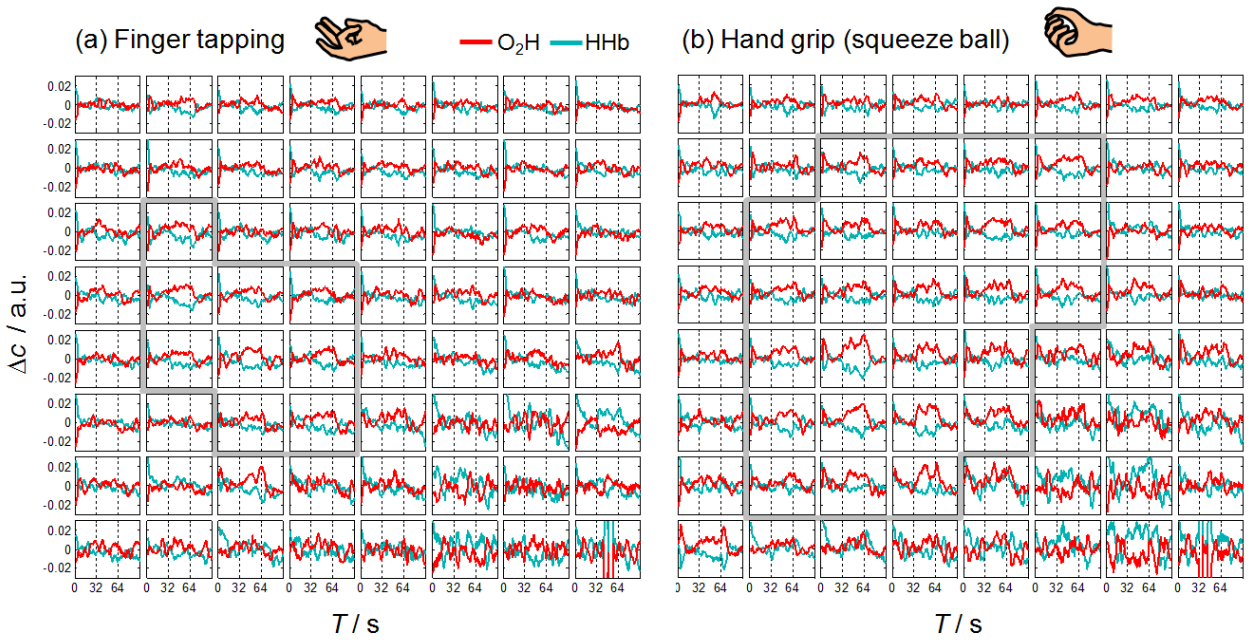

Figure 4. Brain activation in a healthy subject by two different motor tasks (activation for *T* from 32 s to 64 s). The activated regions are indicated by gray margins. The concentration changes in oxy- and deoxyhemoglobin (O_2Hb, HHb) were derived from the gated detection channel. The scan area was 40 mm×40 mm. The original 32×16 pixel image was binned to 8×8 pixels.

5. CONCLUSIONS

We demonstrated that non-contact dynamic imaging of brain activation is feasible. Phantom experiments with localized inclusions and a source-detector separation of 5 mm revealed that the penetration depth was clearly improved when detecting late photons rather than the entire time-of-flight distribution. In-vivo tests, in particular with motor stimulation, yielded a reproducible signal that was indicative of a cerebral hemodynamic activation. Although its applicability is restricted to hairless parts of the body, the non-contact scanning approach may be advantageous for a number of applications where high density functional optical mapping of deep tissues is required or helpful. Examples are the localization of functional activation in the prefrontal cortex, the study of peripheral vascular pathologies or intraoperative monitoring.

ACKNOWLEDGEMENTS

The research leading to these results has received funding from the European Community's Seventh Framework Programme [FP7/2007-2013] under grant agreement n° FP7-HEALTH-F5-2008-201076.

REFERENCES

[1] Torricelli, A., Contini, D., Pifferi, A., Caffini, M., Re, R., Zucchelli, L.., Spinelli, L., "Time domain functional NIRS imaging for human brain mapping," NeuroImage **85 Pt 1**, 28–50 (2014).

[2] Pifferi, A., Torricelli, A., Spinelli, L., Contini, D., Cubeddu, R., Martelli, F., Zaccanti, G., Tosi, A., Dalla Mora, A., et al., "Time-resolved diffuse reflectance using small source-detector separation and fast single-photon gating," Phys. Rev. Lett. **100**(13), 138101 (2008).

[3] Dalla Mora, A., Tosi, A., Zappa, F., Cova, S., Contini, D., Pifferi, A., Spinelli, L., Torricelli, A.., Cubeddu, R., "Fast-Gated Single-Photon Avalanche Diode for Wide Dynamic Range Near Infrared Spectroscopy," Sel. Top. Quantum Electron. IEEE J. Of **16**(4), 1023–1030 (2010).

[4] Mazurenka, M., Jelzow, A., Wabnitz, H., Contini, D., Spinelli, L., Pifferi, A., Cubeddu, R., Dalla Mora, A., Tosi, A., et al., "Non-contact time-resolved diffuse reflectance imaging at null source-detector separation," Opt. Express **20**(1), 283–290 (2012).

[5] Mazurenka, M., Di Sieno, L., Boso, G., Contini, D., Pifferi, A., Mora, A. D., Tosi, A., Wabnitz, H.., Macdonald, R., "Non-contact in vivo diffuse optical imaging using a time-gated scanning system," Biomed. Opt. Express **4**(10), 2257–2268 (2013).

[6] Wabnitz, H., Mazurenka, M., Sieno, L. D., Boso, G., Becker, W., Fuchs, K., Contini, D., Mora, A. D., Tosi, A., et al., "Time-Domain Diffuse Optical Imaging of Tissue by Non-contact Scanning," [Advanced Time-Correlated Single Photon Counting Applications], W. Becker, Ed., Springer International Publishing, 561–585 (2015).

[7] Boso, G., Dalla Mora, A., Della Frera, A.., Tosi, A., "Fast-gating of single-photon avalanche diodes with 200 ps transitions and 30 ps timing jitter," Sens. Actuators Phys. **191**, 61–67 (2013).

[8] Wabnitz, H., Taubert, D. R., Mazurenka, M., Steinkellner, O., Jelzow, A., Macdonald, R., Milej, D., Sawosz, P., Kacprzak, M., et al., "Performance assessment of time-domain optical brain imagers, part 1: basic instrumental performance protocol," J. Biomed. Opt. **19**(8), 086010 (2014).

[9] Wabnitz, H., Jelzow, A., Mazurenka, M., Steinkellner, O., Macdonald, R., Milej, D., Żołek, N., Kacprzak, M., Sawosz, P., et al., "Performance assessment of time-domain optical brain imagers, part 2: nEUROPt protocol," J. Biomed. Opt. **19**(8), 086012 (2014).

[10] Spinelli, L., Botwicz, M., Zolek, N., Kacprzak, M., Milej, D., Sawosz, P., Liebert, A., Weigel, U., Durduran, T., et al., "Determination of reference values for optical properties of liquid phantoms based on Intralipid and India ink," Biomed. Opt. Express **5**(7), 2037–2053 (2014).

[11] Martelli, F., Pifferi, A., Contini, D., Spinelli, L., Torricelli, A., Wabnitz, H., Macdonald, R., Sassaroli, A.., Zaccanti, G., "Phantoms for diffuse optical imaging based on totally absorbing objects, part 1: Basic concepts," J. Biomed. Opt. **18**(6), 066014 (2013).